KONA Powder and Particle Journal No. 38 (2021) 82–93/https://doi.org/10.14356/kona.2021016 Review Paper

Agglomeration and Dispersion Related to Particle Charging in Electric Fields †

Mizuki Shoyama and Shuji Matsusaka *

Department of Chemical Engineering, Kyoto University, Japan

Abstract

Electrostatic forces cause spontaneous movement of charged particles; subsequently, electrostatic technology is attracting attention because of its application in powder handling processes, such as separation, classification, dispersion, and collection. Dielectric and conductive particles are charged by induction in a strong electric field and moved by Coulomb forces. The magnitude and polarity of the transferred charges are controlled by the strength and direction of the electric field. The dielectric particles are also polarized in the electric field, and dipole interactions occur between particles or in the particle layers, complicating the particle behavior. This review paper presents induction charging, agglomeration, levitation, and other behaviors resulting from particle layers in electric fields. A series of particle phenomena occur in parallel electrode systems, which consist of a lower plate electrode and an upper mesh electrode. Charged agglomerates are formed on the particle layers, levitated by the Coulomb forces, and disintegrated with rotation when approaching the mesh electrode. The mechanisms of agglomeration and disintegration have been elucidated in multiple studies, including microscopic observations and theoretical analyses of particle motion, based on numerical calculations of the electric field. Furthermore, a new system is proposed for continuous feeding of dispersed particles using electric fields and vibration.

Keywords: particle, electric field, charging, agglomeration, levitation, dispersion

1. Introduction

In powder handling processes, the deposition of charged particles is a common phenomenon. The accumulation of charged particles on surfaces reduces operability and leads to lower productivity; thus, charged particles must be removed from the surfaces. Fluid flow (Masuda et al., 1994; Gotoh et al., 2015) and vibration (Kobayakawa et al., 2015; Adachi et al., 2017) are effective for removing particles. Another effective method is the application of external electric fields, which enables remote control of the motion of charged particles (Masuda et al., 1972; Calle et al., 2009; Kawamoto et al., 2011). Dielectric particles and conductive particles can be charged by induction in a strong electric field and moved by Coulomb forces. The magnitude and polarity of the transferred charge are controlled by the strength and direction of the electric field. The dielectric particles are also polarized in the electric field, and dipole interactions act between the particles or in the particle layers; thereby, the particle behavior becomes more complicated.

The induction charging, agglomeration, levitation, and other behaviors resulting from particle layers in electric fields have been studied in detail (Shoyama and Matsusaka, 2017, 2019; Shoyama et al., 2019). Furthermore, a new system has been proposed for the continuous feeding of dispersed particles using electric fields and vibration (Shoyama et al., 2018). Based on previous studies, this review paper summarizes the mechanisms of induction charging, the control of particle behavior, and the concept of its application.

2. Induction charging of single particles

When a conductive particle comes into contact with an inside wall of a parallel electrode with a different polarity, the particle is charged to the same polarity as the electrode. This phenomenon is called induction charging (Blanchard, 1958; Cho, 1964). Charges cannot pass through ideal dielectric materials; however, dielectric materials have a low degree of conductivity on the surface or in the body. Thus, various types of particles can be charged by induction.

The equilibrium charge of a conductive particle by induction is represented by (Cho, 1964)

† Received 13 June 2020; Accepted 28 July 2020
J-STAGE Advance published online 5 September 2020
* Corresponding author: Shuji Matsusaka;
Add: Kyoto 615-8510, Japan
E-mail: matsu@cheme.kyoto-u.ac.jp
TEL: +81-75-383-3054 FAX: +81-75-383-3054

$$q_\infty = 1.65\pi\varepsilon_{rf}\varepsilon_0 D_p^2 E_{ex} \quad (1)$$

where ε_{rf} is the relative permittivity of the fluid, ε_0 is the vacuum permittivity, D_p is the particle diameter, and E_{ex} is the external electric field strength.

The equilibrium charge of a dielectric particle is represented by (Wu et al., 2003)

$$q_\infty = 0.55p\pi\varepsilon_{rf}\varepsilon_0 D_p^2 E_{ex} \quad (2)$$

and

$$p = \frac{3\varepsilon_{rp}}{\varepsilon_{rp}+2} \quad (3)$$

where ε_{rp} is the relative permittivity of the particle. The particle charge as a function of time is expressed as

$$q_p(t) = q_{pe}[1-\exp(-t/\tau)] \quad (4)$$

and

$$\tau = \rho_v\varepsilon_0\varepsilon_{rp} \quad (5)$$

where ρ_v is the volume resistivity of the particle.

3. Motion of charged particles between parallel electrodes and other applications

Particles sufficiently charged by induction can be made to levitate from the electrode by Coulomb forces, and then move toward the counter electrode. When the particles come into contact with the counter electrode, their polarity is inverted. Consequently, the particles move back to the first electrode and then oscillate between the electrodes (Cho, 1964). Highly conductive particles are charged immediately after contact with the electrodes. For low conductivity particles, charging takes time (Ohkubo and Takahashi, 1996a, 1996b; Wu et al., 2003; Nader et al., 2009). However, if electrical resistance is extremely high, induction charging will not occur. Instead, contact charging will dominate (Matsusaka et al., 2010; Matsusaka, 2011). As the quantity of charge transferred by one contact charging event is rather small, particles involved in contact charging cannot be levitated.

In the above system, there can be both positively and negatively charged particles between electrodes. To extract unipolar charged particles, openings may be required in one of the parallel electrodes. Replacing the upper plate electrode with a mesh electrode allows the passage of unipolar charged particles through the openings (Tada et al., 2004). When charged particles with the same polarity are extracted from the revised system, these particles are dispersed by their mutual electrostatic repulsion (Masuda, 2009).

There are many electrostatic applications for the control of particle position (Matsusaka et al., 2008), separation (Dwari et al., 2015), classification (Kawamoto, 2008), and surface cleaning (Mazumder et al., 2007; Kawamoto et al., 2011). In addition, there are reports regarding particle levitation using various configurations of electrodes (Adachi et al., 2016; Blajan et al., 2017). These electric fields allow particles to move even in the absence of mechanical and/or pneumatic systems. Thus, electrostatic techniques are expected to be used in various fields such as space exploration (Kawamoto et al., 2011; Adachi et al., 2016), and under atmospheric pressure.

4. Agglomeration and levitation in electric fields

Dielectric particles are polarized in an electric field and tend to form chain agglomerates along the direction of the electric field because of the interactions between polarized particles (Hollmann, 1950; Pearce, 1954; Nakajima and Matsuyama, 2002). The interaction between dipoles is illustrated in **Fig. 1**. A typical example of the application of this interaction is an electrorheological fluid (ERF), which is a suspension of dielectric particles dispersed in an insulating liquid. The ERF changes apparent viscosity by forming chain-like structures of particles (Parthasarathy and Klingenberg, 1996).

Shoyama and Matsusaka (2017) conducted experiments on the behavior of particles (glass beads: D_{p50} = 100 μm) in gases using parallel electrodes at a distance of 10 mm. **Fig. 2** schematically shows the experimental setup. Particle layers with a thickness of 1 mm are placed on the lower electrode, which is connected to a power supply, and the upper electrode is grounded. The behavior of the particles in the external electric field is recorded by a high-speed camera with a zoom lens.

When the voltage of the lower electrode is set to V_L = 5 kV, single particles and chain agglomerates levitate from the particle layers, as shown in **Fig. 3**. These phenomena can be explained as follows. (1) The dielectric particles

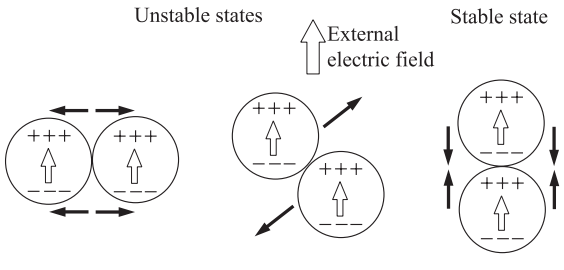

Fig. 1 Interaction between dipoles.

(glass beads) are polarized in the upward electric field. (2) As mutual electrostatic interactions act between the particles, chain agglomerates are formed. (3) As the particle surfaces have a relatively low conductivity, the electrons move downward due to induction; consequently, the particles on the top surface of the particle layers are positively charged. (4) The charged particles experience upward Coulomb forces in the electric field. (5) As the Coulomb forces overcome the downward forces, the particles levitate.

Fig. 4a shows a simulation model for electric field calculation using FEM (COMSOL Multiphysics, COMSOL, Inc.). A chain agglomerate is placed on the top surface of 1-mm-thick particle layers in a 3D Cartesian coordinate system (x, y, z). The calculation domain is set to 5 D_p × $3\sqrt{3}$ D_p for the horizontal cross section and 10 mm for the height, which is the same as the distance between the electrodes in the experimental setup. The top and bottom boundaries are set to zero and a given voltage, respectively. Periodic boundary conditions are applied at the side boundaries. The charges of the agglomerate and the top particle layer are given based on the experimental result. The relative permittivity of the particles is also given for the calculation.

Fig. 4b shows the calculated electric field strength E_{exz} in the z-direction. The E_{exz} value in the region of $z < 1$ mm is almost zero in an electrostatic equilibrium state, although there are small fluctuations caused by particle arrangements. In contrast, the E_{exz} values within the agglomerate (z = 1 – 1.18 mm) are relatively high and fluctuate significantly at the particle contact points and on the top of the agglomerate.

Fig. 5 shows a series of images of a levitated particle at intervals of 2 ms. The particle moves upward, accelerating in the electric field. **Fig. 6** shows a series of images of agglomeration and levitation at intervals of 10 ms. The polarized particles form a straight-chain agglomerate by mutual electrostatic interactions, and the agglomerate levitates at 60 ms.

Particle charge can be calculated based on the motion analysis of levitated particles. A straight-chain agglomerate moving in an electric field experiences a drag force $\boldsymbol{F}_d$, a gravitational force $\boldsymbol{F}_g$, and an electrostatic force $\boldsymbol{F}_e$. The equation of motion of the agglomerate is expressed as

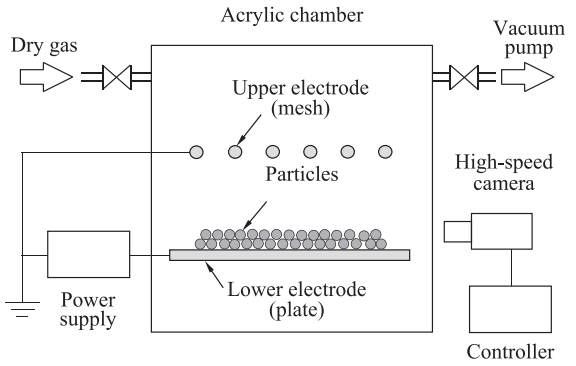

Fig. 2 A parallel electrode system.

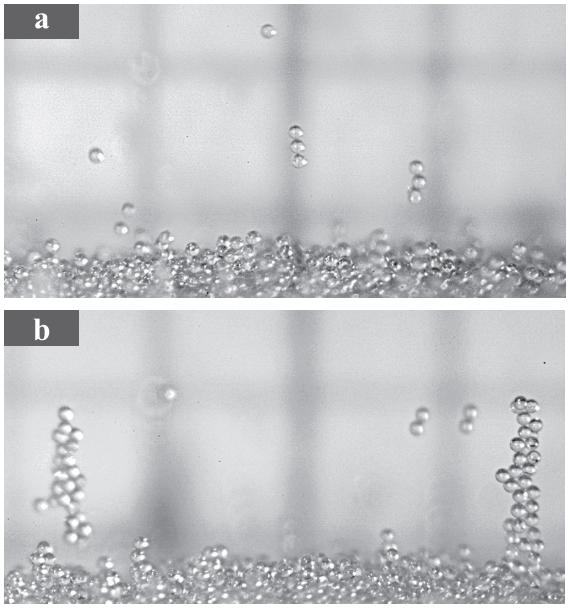

Fig. 3 Snapshots: **(a)** levitation of single particles and chain agglomerates and **(b)** formation of large agglomerates (glass beads: D_{p50} = 100 µm, ρ_p = 2300 kg/m^3, ε_{rp} = 7).

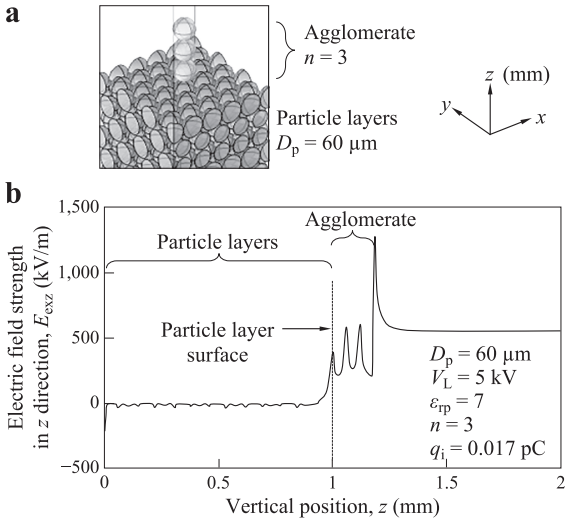

Fig. 4 Electric field calculation using FEM: **(a)** simulation model and **(b)** calculated values along the axis of the chain agglomerate.

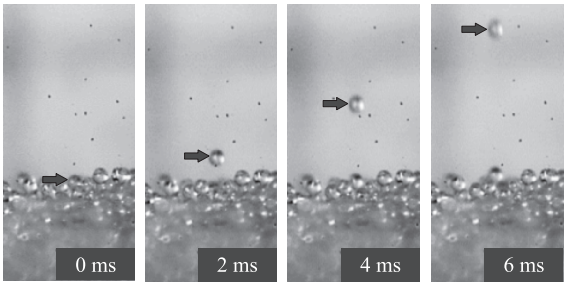

Fig. 5 Levitation of a single particle (glass beads: D_{p50} = 100 µm).

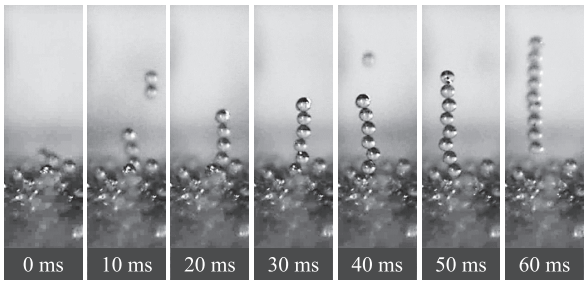

Fig. 6 Agglomeration and levitation (glass beads: D_{p50} = 100 μm).

$$nm_p \frac{d\boldsymbol{v}_a}{dt} = \boldsymbol{F}_d + \boldsymbol{F}_g + \boldsymbol{F}_e \tag{6}$$

where n is the number of the primary particles constituting the agglomerate, m_p is the mass of each primary particle, $\boldsymbol{v}_a$ is the velocity of the agglomerate, and t is time. The mass of each particle is defined as

$$m_p = \frac{\pi D_p{}^3 \rho_p}{6} \tag{7}$$

where ρ_p is particle density. For a stationary fluid, $\boldsymbol{F}_d$ is given by (Kasper et al., 1985; Niida and Ohtsuka, 1997)

$$\boldsymbol{F}_d = 3\pi\mu D_a \boldsymbol{v}_a \kappa \tag{8}$$

where μ is the viscosity of the fluid and D_a is the volume equivalent diameter of the agglomerate, which is defined as

$$D_a = n^{\frac{1}{3}} D_p \tag{9}$$

κ is the dynamic shape factor given by

$$\frac{1}{\kappa} = \frac{1}{\kappa_\perp} + \left(\frac{1}{\kappa_{/\!/}} - \frac{1}{\kappa_\perp}\right)\cos^2\theta_m \tag{10}$$

where θ_m is the angle between the agglomerate axis and the moving direction. $\kappa_\perp$ and $\kappa_{/\!/}$ are the dynamic shape factors perpendicular and parallel to the moving direction, respectively. That is,

$$\kappa_\perp = \begin{cases} 1.00 & (n=1) \\ 1.16 & (n=2) \\ 1.26 & (n=3) \end{cases} \tag{11}$$

and

$$\kappa_{/\!/} = \begin{cases} 1.00 & (n=1) \\ 1.03 & (n=2) \\ 1.07 & (n=3) \end{cases} \tag{12}$$

The gravitational force of the agglomerate is defined as

$$\boldsymbol{F}_g = n m_p \boldsymbol{g} \tag{13}$$

where $\boldsymbol{g}$ is gravitational acceleration. When the agglomerate is close to an object, such as the surface of the particle layers, the electrostatic force $\boldsymbol{F}_e$ consists of the Coulomb force $\boldsymbol{F}_{ex}$ in the external electric field, the image force $\boldsymbol{F}_i$, the interaction force $\boldsymbol{F}_p$ between polarized particles, and the gradient force $\boldsymbol{F}_{grad}$ in a non-uniform electric field (Morgan and Green, 1997). That is,

$$\boldsymbol{F}_e = \boldsymbol{F}_{ex} + \boldsymbol{F}_i + \boldsymbol{F}_p + \boldsymbol{F}_{grad} \tag{14}$$

Here, $\boldsymbol{F}_{ex}$ is expressed as

$$\boldsymbol{F}_{ex} = \sum_{i=1}^{n} \boldsymbol{F}_{qi} \tag{15}$$

where $\boldsymbol{F}_{qi}$ is the Coulomb force acting on the i-th particle in the agglomerate, which is defined as

$$\boldsymbol{F}_{qi} = q_i \boldsymbol{E}_{ex} \tag{16}$$

where q_i is the charge of the i-th particle, and $\boldsymbol{E}_{ex}$ is the external electric field. $\boldsymbol{F}_i$ is expressed as (Weber, 1950)

$$\boldsymbol{F}_i = \frac{1}{16\pi\varepsilon_{rf}\varepsilon_0} \cdot \frac{\varepsilon_{rs} - \varepsilon_{rf}}{\varepsilon_{rs} + \varepsilon_{rf}} \sum_{i=1}^{n} \frac{q_i^2}{z_{pi}^2} \tag{17}$$

where ε_{rs} is the relative permittivity of the particle layers, and z_{pi} is the position of the i-th particle on the top surface of the particle layers in the z-direction. When the axis of the chain agglomerate is parallel to the external electric field, $\boldsymbol{F}_p$ is expressed as (Parthasarathy and Klingenberg, 1996)

$$\boldsymbol{F}_p = \frac{3}{8}\pi\varepsilon_0\varepsilon_{rf}\left(\frac{\varepsilon_{rp}-1}{\varepsilon_{rp}+2}\right)^2\left(\frac{D_p}{d}\right)^4 D_p^2 \boldsymbol{E}_{ex}^2 \tag{18}$$

where ε_{rp} is the relative permittivity of the particle. $\boldsymbol{F}_{grad}$ is expressed as (Hywel and Green, 1997)

$$\boldsymbol{F}_{grad} = \frac{1}{4}\pi\varepsilon_0\varepsilon_{rf}\frac{\varepsilon_{rp}-1}{\varepsilon_{rp}+2} D_a^3 \,\mathrm{grad}\, \boldsymbol{E}_{ex}^2 \tag{19}$$

Fig. 7 shows the experimental data (circles) regarding the position of the levitated particle in the vertical direction z shown in **Fig. 5**. The solid lines in this figure are particle trajectories calculated using Eq. (6). The experimental data agree well with the solid line calculated with a charge of

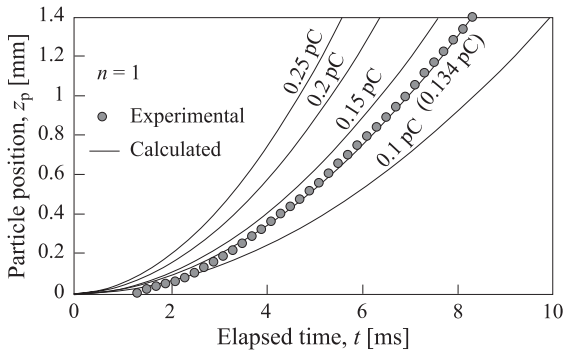

Fig. 7 Particle position as a function of elapsed time with a parameter of particle charge (glass beads: D_{p50} = 100 μm).

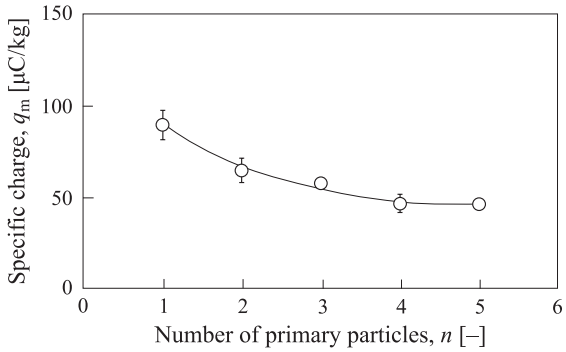

Fig. 8 Relationship between specific charge and the number of primary particles in levitating agglomerate (glass beads: D_{p50} = 100 μm).

0.134 pC, which is 58 % of the value calculated using Eq. (1) and 75 % of the value calculated using Eq. (2). The charge of a particle levitated from particle layers is generally smaller than the charge of a particle levitated from an electrode because of the difference of ε_{rs} in Eq. (17).

Fig. 8 shows the relationship between specific charge, q_m (= q/m_p), and the number of primary particles constituting a levitated agglomerate ($n \geq 2$) or a single particle ($n = 1$). The q_m value decreases with an increase in n. When the charge of the single particle is small, that is, the Coulomb force is small, the particle cannot be levitated. However, when the magnitude of the total Coulomb force of the constituent primary particles is large, the agglomerate can be levitated from the particle layers.

5. Effects of particle characteristics on agglomeration and levitation

Fig. 9 shows the images of particles levitated from different types of particle layers. The applied electric voltage is V_L = 5 kV. For the glass beads (**Fig. 9a**) and alumina particles (**Fig. 9b**), large numbers of both single particles and chain agglomerates are levitated. In contrast, for the ferrite particles (**Fig. 9c**), very few chain agglomerates are levitated. This difference is mainly caused by the electrical resistances of the particles. In cases of low electrical resistance (ferrite particles: ρ_v = 0.8 Ω·m), particles are immediately charged up by induction before forming agglomerates, resulting in single-particle levitation. However, when there is high electrical resistance (glass beads: $\rho_v = 1.1 \times 10^7$ Ω·m; alumina particles: $\rho_v = 0.3 \times 10^6$ Ω·m), particles take time to be charged; in the meantime, chain agglomerates are formed on the particle layers. Although the relative permittivity also affects the relaxation time of charge transfer, as shown in Eqs. (4) and (5), the difference in materials is small (glass beads: ε_{rp} = 7; alumina particles: ε_{rp} = 8.5; ferrite particles: ε_{rp} = 2.2). The effect of the applied voltage on the agglomeration is also small, fitting within a range of V_L = 4 – 6 kV.

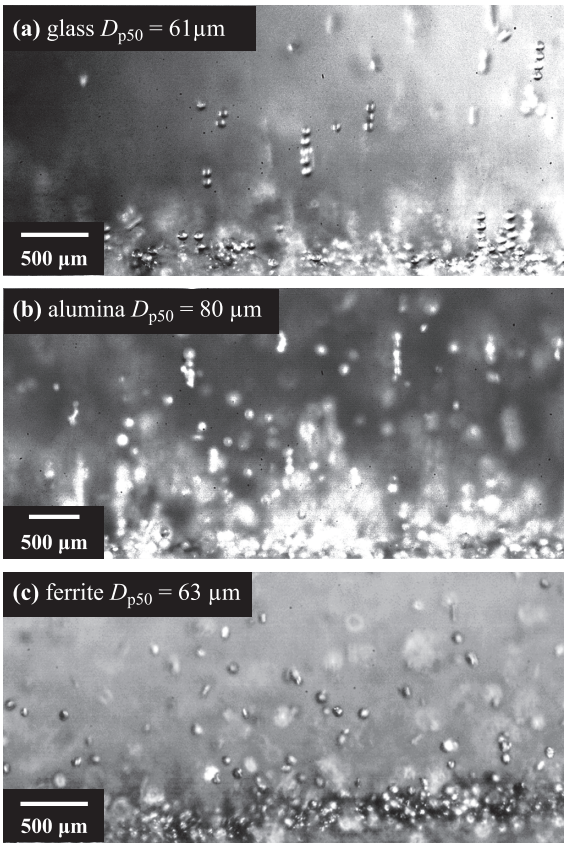

Fig. 9 Images of particles levitated from particle layers at V_L = 5 kV.

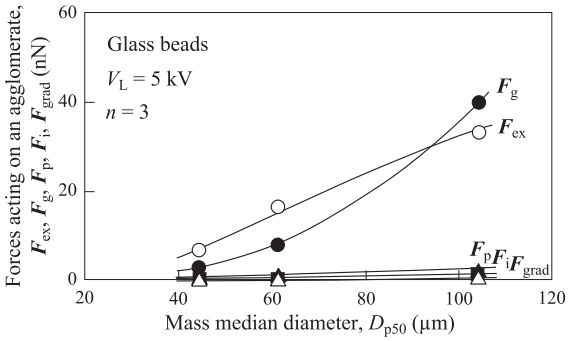

Fig. 10 Forces acting on a charged agglomerate just prior to its separation from particle layers.

To analyze the condition of levitation, the forces acting on agglomerates on the top surface of the particle layers should be studied. **Fig. 10** shows the forces calculated from the experimental values of particle diameter, particle charge, and other physical properties for n = 3. Although the polarization force $\boldsymbol{F}_p$, image force $\boldsymbol{F}_i$, and gradient force $\boldsymbol{F}_{grad}$ are small, the Coulomb force $\boldsymbol{F}_{ex}$ and gravitational force $\boldsymbol{F}_g$ are significantly large. That is, the dominant upward and downward forces are $\boldsymbol{F}_{ex}$ and $\boldsymbol{F}_g$, which increase as a function of particle diameter. These analytical results indicate that the concept of force balance is valid within a permissible error.

6. Disintegration of agglomerates in non-uniform electric fields

The motion of charged particles is changed in a non-uniform electric field. **Fig. 11a** shows an electric field generated by parallel electrodes, which consist of the plate electrode and mesh electrode. The electrode configuration for the simulation is the same as those used in the experiment (see **Fig. 2**). The lines and arrows in this figure indicate the electric potential and electric field direction, respectively. The electric field is uniform in the lower area but non-uniform in the upper area. **Fig. 11b** shows the details of the upper area, indicating that the non-uniform electric field is directed to the center of the wire of the mesh electrode.

Fig. 12a shows a series of images of a chain agglomerate passing through the mesh electrode. The agglomerate consisting of three primary particles moves upward, but its velocity decreases with an increase in height. During this movement, the agglomerate changes its state. **Fig. 12b** shows enlarged images of the same agglomerate. The agglomerate is in a straight-chain structural state at the beginning. From top to bottom, the three primary particles are denoted as P1, P2, and P3, respectively. After the agglomerate begins to rotate counterclockwise, P3 separates from it and moves upward and to the right. The agglomerate consisting of the two primary particles continue to rotate counterclockwise; finally, P1 separates from P2. The probability of disintegration generally increases as a function of the number of constituent primary particles.

When the forces acting on each primary particle in the agglomerate are not the same, the agglomerate experiences the forces in the circumferential as well as in the radial direction. **Fig. 13** illustrates the rotation models in an electric field $\boldsymbol{E}_{ex}$ for $n = 2$ and 3, respectively. θ is the angle of the agglomerate axis relative to the vertical, and φ is the angle between the agglomerate axis and the electric field direction. That is,

$$\varphi = \theta - \theta_{ex} \tag{20}$$

where θ_{ex} is the angle of the external electric field direction at the position of the agglomerate relative to the vertical.

Fig. 14 illustrates the torques acting on chain agglomerates with different values of φ. Here, it is assumed that the charge q_1 for the upper particle is larger than the charge q_2 for the lower particle at $\varphi = 0$. The larger charge generates a stronger Coulomb force; thus, the agglomerate experiences a torque ($\boldsymbol{T}_q$) around the centroid. The agglomerate also experiences a torque ($\boldsymbol{T}_p$) caused by the dipole interactions

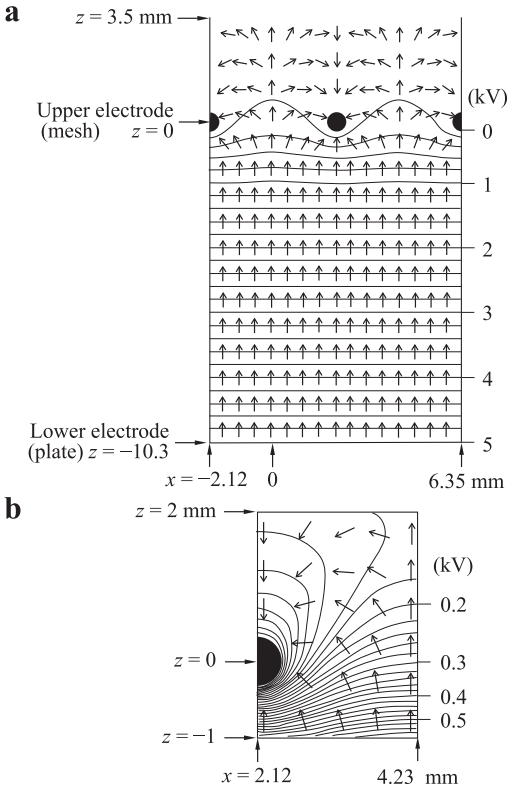

Fig. 11 Calculated electric field: **(a)** overview and **(b)** enlarged view.

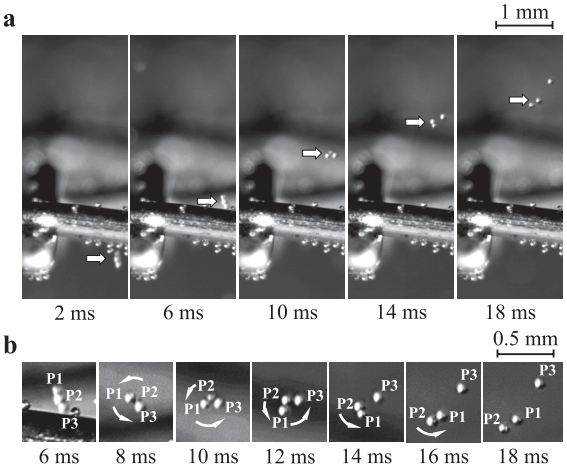

Fig. 12 Disintegration of a chain agglomerate passing through the mesh electrode: **(a)** fixed-point images and **(b)** enlarged images of the agglomerate (glass beads: D_{p50} = 100 μm).

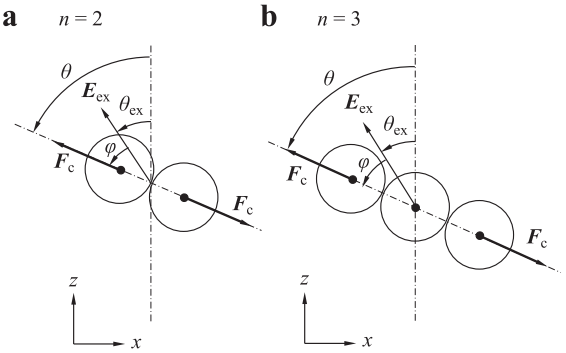

Fig. 13 Rotation model of chain agglomerates in an electric field **(a)** $n = 2$ and **(b)** $n = 3$.

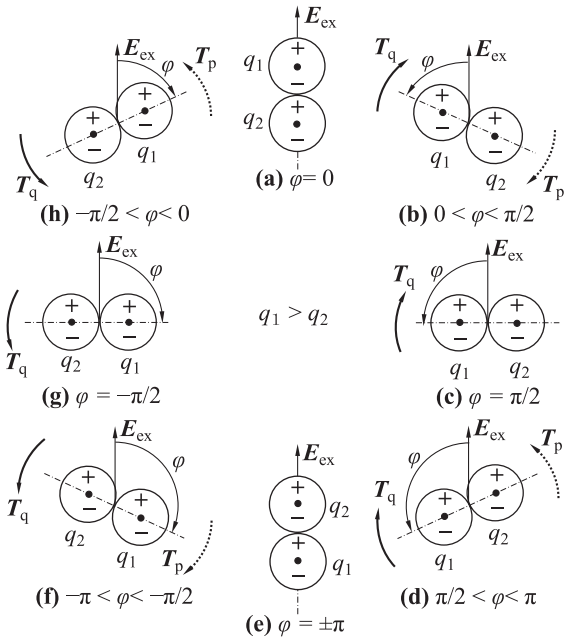

Fig. 14 Torques acting on chain agglomerates (n = 2).

in the electric field. $\boldsymbol{T}_{\mathrm{p}}$ allows the particle axis to align with the electric field direction.

Furthermore, an agglomerate consisting of n primary particles experiences a torque ($\boldsymbol{T}_{\mathrm{d}}$) caused by the drag forces during rotation; therefore, the equation for rotational motion is expressed as

$$I\frac{\mathrm{d}\boldsymbol{\omega}}{\mathrm{d}t}=\boldsymbol{T}_{\mathrm{q}}+\boldsymbol{T}_{\mathrm{p}}+\boldsymbol{T}_{\mathrm{d}} \tag{21}$$

where I is the moment of inertia given by

$$I=\sum_{i=1}^{n} m_{\mathrm{p}} r_i^{\,2} \tag{22}$$

where r_i is the particle position relative to the axis of rotation, and $\boldsymbol{\omega}$ is the angular velocity. The magnitude of ω is given by

$$\omega=\frac{\mathrm{d}\theta}{\mathrm{d}t} \tag{23}$$

The torque $\boldsymbol{T}_{\mathrm{q}}$ around the centroid caused by Coulomb forces is given by

$$\boldsymbol{T}_{\mathrm{q}}=\sum_{i=1}^{n}\left(\boldsymbol{F}_{\mathrm{q}i}\times\boldsymbol{r}_i\right) \tag{24}$$

The interaction force $\boldsymbol{F}_{\mathrm{p}ij}$ between particles polarized in the electric field was defined by Klingenberg et al. (1989) and Washizu and Jones (1994). They considered an induced field caused by the existence of the particles in the electric field. A simple model was also presented by Klingenberg et al. (1989) and Parthasarathy and Klingenberg (1996). Using this simple model, the electrostatic interaction force $\boldsymbol{F}_{\mathrm{p}ij}$ between the i-th and j-th particles is determined as

$$\boldsymbol{F}_{\mathrm{p}ij}=F_0\left(\frac{D_{\mathrm{p}}}{r_{ij}}\right)^4\left\{\left(3\cos^2\varphi-1\right)\boldsymbol{e}_r+\sin 2\varphi\boldsymbol{e}_\varphi\right\} \tag{25}$$

where r_{ij} is the distance between the two particle centroids. $\boldsymbol{e}_r$ and $\boldsymbol{e}_\varphi$ are unit vectors in the radial and circumferential directions, respectively. F_0 is expressed as

$$F_0=\frac{3}{16}\pi\varepsilon_0\varepsilon_{\mathrm{rf}}D_{\mathrm{p}}^{\,2}\left(\frac{\varepsilon_{\mathrm{rp}}-1}{\varepsilon_{\mathrm{rp}}+2}\right)^2 E_{\mathrm{ex}}^2 \tag{26}$$

The first and second terms on the right-hand side of Eq. (25) represent the electrostatic interaction forces in the radial and circumferential directions, respectively. Therefore, the force acting on the i-th particle due to the other particles $\boldsymbol{F}_{\mathrm{p}\varphi i}$ in the circumferential direction is given by

$$\boldsymbol{F}_{\mathrm{p}\varphi i}=\sum_{j=1}^{n}F_0\left(\frac{D_{\mathrm{p}}}{r_{ij}}\right)^4\sin 2\varphi\,\boldsymbol{e}_\varphi \qquad (j\neq i) \tag{27}$$

Torque $\boldsymbol{T}_{\mathrm{p}}$ caused by dipole interactions in the electric field is given by

$$\boldsymbol{T}_{\mathrm{p}}=\sum_{i=1}^{n}\left(\boldsymbol{F}_{\mathrm{p}\varphi i}\times\boldsymbol{r}_i\right) \tag{28}$$

In the same manner, torque $\boldsymbol{T}_{\mathrm{d}}$ caused by the drag forces is given by

$$\boldsymbol{T}_{\mathrm{d}}=\sum_{i=1}^{n}\left(\boldsymbol{F}_{\mathrm{d}i}\times\boldsymbol{r}_i\right) \tag{29}$$

where $\boldsymbol{F}_{\mathrm{d}i}$ is the drag force of the i-th primary particle as a function of the velocity $\mathbf{v}_{\mathrm{p}}$. That is,

$$\boldsymbol{F}_{\mathrm{d}i}=3\pi\mu D_{\mathrm{p}}\boldsymbol{v}_{\mathrm{p}i} \tag{30}$$

The rotation of the agglomerate can be calculated using Eq. (21). The angular velocity increases as a function of the spread of charge distribution in the agglomerate. Charge distribution is generally caused by electrostatic induction during levitation in the external electric field. The rotation generates centrifugal force, which can cause the disintegration of the agglomerate. The centrifugal force $|F_{\mathrm{c}}|$ acting on a constituent primary particle is given by

$$|F_{\mathrm{c}}|=m_{\mathrm{p}}\,r\,\omega^2 \tag{31}$$

Fig. 15 shows the temporal variation of the adhesion force $|F_{\mathrm{a}}|$ and centrifugal force $|F_{\mathrm{c}}|$ based on the actual particle behavior (see **Fig. 12**). The values of $|F_{\mathrm{a}}|$ and $|F_{\mathrm{c}}|$ are calculated using the first term on the right-hand side of Eq. (25) and Eq. (31), respectively. $|F_{\mathrm{a}}|$ is initially high but decreases with time, whereas $|F_{\mathrm{c}}|$ increases with time for both n = 3 and n = 2. Particle separation is initiated at 10 and 15 ms when $|F_{\mathrm{c}}| > |F_{\mathrm{a}}|$ is satisfied. This implies that the centrifugal force plays a significant role in agglomerate disintegration in the non-uniform electric field.

7. Continuous feeding of dispersed particles

In powder handling processes, continuous feeding and the control of particle motion are essential for stable operation and the quality control of products. To realize these operations, a conceptual system using electric fields and vibration has been proposed (Matsusaka et al., 2013; Kawamoto et al., 2016). This system can also be applied to the electrostatic characterization of particles, where the particles are charged by the contact potential difference (Mizutani et al., 2015). Shoyama et al. (2018) have developed a new system for continuous particle feeding and dispersion using both parallel electrodes and a vibrator. The experimental setup is schematically shown in **Fig. 16**. A mesh electrode is placed at a distance of 20 mm from the plate electrode, which is attached to an inclined acrylic base. One of the electrodes is connected to a DC power supply, and the other electrode is grounded. Particles are fed at a constant flow rate and transported on the lower electrode, which is vibrated to improve particle flowability.

Fig. 17 shows images of particle behaviors observed at different applied voltages. The particles are levitated from the lower electrode and widely dispersed. When voltage is applied to the upper electrode, the particles are more widely spread than when a voltage is applied to the lower electrode. The spread area of the particles increases as a function of the absolute value of the applied voltage.

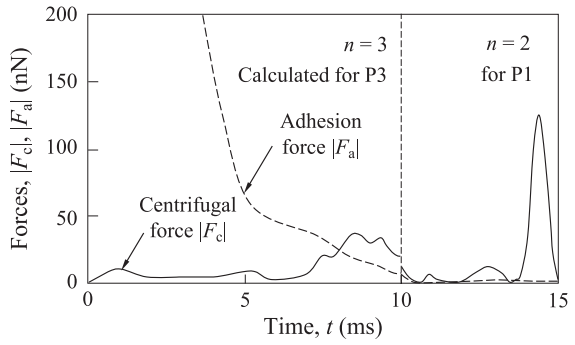

Fig. 15 Comparison between centrifugal force and adhesion force (glass beads: $D_{p50} = 100$ μm).

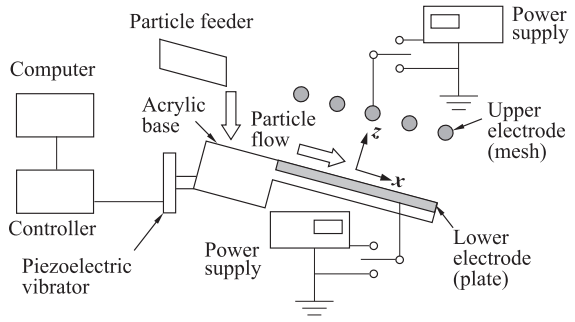

Fig. 16 Experimental setup for continuous feeding of dispersed particles.

Fig. 18 shows the quantitative analysis of particle dispersion for different applied voltages. For $V_U = 0$ and $V_L > 0$ (**Fig. 18a**), the range of particle position increases as a function of the value of V_L, and the distributions are monomodal. As for $V_L = 0$ and $V_U < 0$ (**Fig. 18b**), the distributions are bimodal, and the range is obviously wider.

Fig. 19 illustrates the concept of the charging and the motion of particles in this system. The upper virtual boundary is assumed to be zero. For $V_U = 0$ and $V_L > 0$ (**Fig. 19a**), the electric field below the upper electrode is directed upward. Particles that are positively charged on the lower electrode experience upward Coulomb forces. The levitated

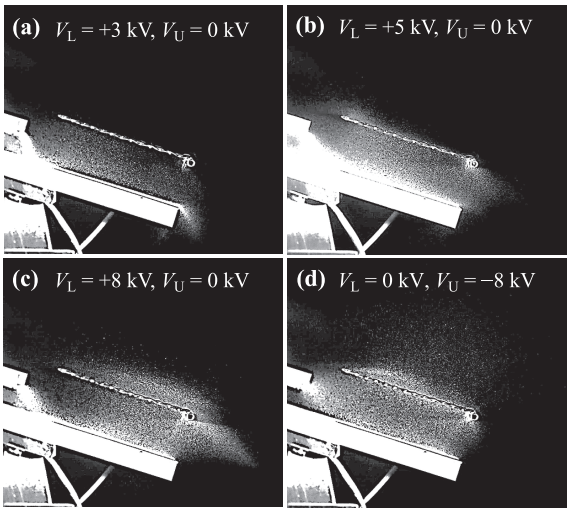

Fig. 17 Effect of applied voltage on particle dispersion (alumina particles: $D_{p50} = 48$ μm, $\rho_p = 3800$ kg/m^3).

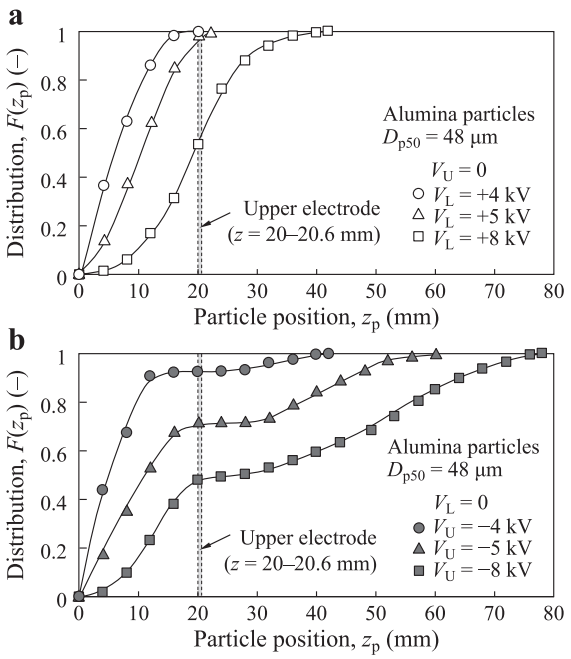

Fig. 18 Quantitative analysis of particle dispersion in the z-direction (alumina: $D_{p50} = 48$ μm): **(a)** $V_U = 0$ and $V_L > 0$; and **(b)** $V_L = 0$ and $V_U < 0$.

particles can pass through the mesh electrode due to particle inertia. However, there are limits to the maximum heights of the particles under the effect of the gravitational forces; thus, these particles are attracted to the upper electrode. After adhesion, their polarity is changed by induction charging. The negatively charged particles levitate from the upper electrode. However, the Coulomb forces above the upper electrode drastically decrease with increasing height; therefore, the particles cannot reach higher positions. The polarities in **Fig. 19b** are opposite to those in **Fig. 19a**; however, the motions of the particles are the same.

When $V_U < 0$ (**Fig. 19c**), two electric fields are formed; one is directed upward below the upper electrode, and the other is directed downward above this electrode. Once the particles adhere to the upper electrode, their polarity changes. As the Coulomb forces above the upper electrode are directed upward, the particles can reach higher positions. Consequently, the polarity of the charged particles at the higher position is opposite to that of the particles levitated from the lower electrode. The polarities in **Fig. 19d** are opposite to those in **Fig. 19c**; however, the motions of the particles are the same.

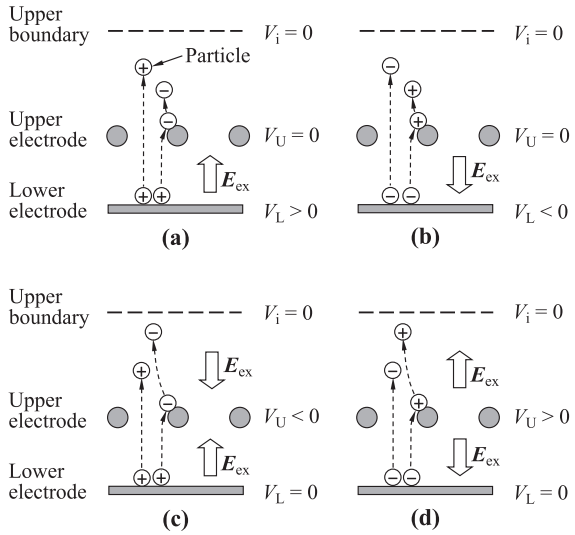

Fig. 19 Concept of the charging and the motion of particles in this system: **(a)** $V_U = 0$ and $V_L > 0$; **(b)** $V_U = 0$ and $V_L < 0$; **(c)** $V_L = 0$ and $V_U < 0$; **(d)** $V_L = 0$ and $V_U > 0$.

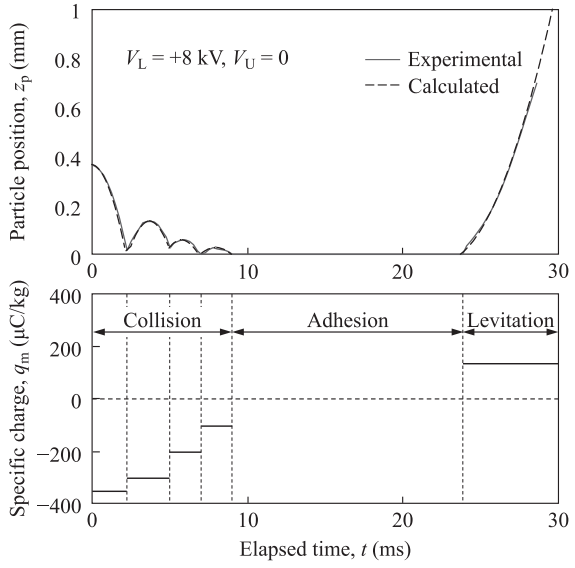

Fig. 20 A series of a particle's motions on the lower electrode and the specific charge of the particle (alumina: D_{p50} = 48 μm, V_L = +8 kV and V_U = 0).

The polarity of charged particles is changed by the conditions; thus, some particles repeatedly collide with the electrodes. **Fig. 20** shows a series of a particle's motions on the lower electrode and the specific charge of the particle q_m. The upper figure indicates the particle position in the z-direction as a function of time. The experimental results (solid lines) agree well with the calculated results based on the equation of motion (broken lines). The lower figure indicates the variation of the specific charge estimated from the motion analysis. The particle motion can be classified into three categories, namely, collision, adhesion, and levitation. In the collision process, the charged particle is attracted to the lower electrode by the Coulomb force and repeatedly collides with decreasing rebound height. The absolute value of the negative charge of the particle decreases with the number of collisions because the particle acquires some positive charge during each collision. After losing its kinetic energy, the particle adheres to the lower electrode. As the particle acquires a larger positive charge by induction charging for a period of 15 ms, the polarity of the particle is changed to positive. When the Coulomb force becomes sufficiently large, the particle is levitated again. Here, it is worth noting that the transferred charge depends on the contact time.

8. Conclusions

This review paper presents a series of particle phenomena occurring in parallel electrode systems consisting of a lower plate electrode and an upper mesh electrode. Particle layers are placed on the plate electrode. The mechanisms of induction charging, the control of particle behavior, and the concept of its application are summarized as follows:

(1) Particles on the top surface of the particle layers are charged by induction in a strong electric field even though the particles are dielectric. These particles are also polarized and form a straight-chain agglomerate on the particle layers by mutual electrostatic interactions.

(2) Single particles and agglomerates can be levitated from the particle layers by Coulomb forces. When the charge of single particles is relatively small, the particles are not levitated. However, when the magnitude of the total Coulomb force of the constituent primary particles is large, the agglomerates can be levitated. The charge of the

primary particles decreases with an increase in the number of primary particles in the agglomerate.
(3) In situations of low electrical resistance, particles are immediately charged up by induction. When there is high electrical resistance, particles take time to be charged. Therefore, in the former, single particles are easily levitated because of excessive charges on the surfaces. As for the latter, agglomerates tend to be levitated.
(4) Levitated agglomerates disintegrate with rotation when approaching the mesh electrode. The rotation is controlled by the torque, which is caused by the charge distribution in the agglomerates. The rotation generates a centrifugal force, which acts as a separation force.
(5) A new system is proposed for the continuous feeding of dispersed particles using electric fields and vibration. Particle charge depends on the contact time of the electrode. When voltage is applied to the upper electrode, particles are more widely spread above the electrode than when a voltage is applied to the lower electrode. The spread area of the particles increases as a function of the absolute value of the applied voltage.

Nomenclature

D_a	volume equivalent diameter of agglomerate (m)
D_p	particle diameter (m)
D_{p50}	mass median diameter (m)
$\boldsymbol{E}_{ex}$	external electric field (V/m)
E_{exz}	external electric field strength in the z-direction (V/m)
$\boldsymbol{e}$	unit vector (–)
$\lvert F_a \rvert$	magnitude of adhesion force (N)
$\lvert F_c \rvert$	magnitude of centrifugal force (N)
$\boldsymbol{F}_d$	drag force (N)
$\boldsymbol{F}_e$	electrostatic force (N)
$\boldsymbol{F}_{ex}$	Coulomb force in external electric field (N)
$\boldsymbol{F}_g$	gravitational force (N)
$\boldsymbol{F}_{grad}$	gradient force (N)
$\boldsymbol{F}_i$	image force (N)
$\boldsymbol{F}_p$	interaction force between polarized particles (N)
$\boldsymbol{F}_{pij}$	interaction force between i-th and j-th particles polarized in electric field (N)
$\boldsymbol{F}_q$	Coulomb force acting on primary particle (N)
$F(z_p)$	cumulative distribution of particle positions in the z-direction (–)
$\boldsymbol{g}$	gravitational acceleration (m/s^2)
I	moment of inertia (kg·m^2)
m_p	mass of primary particle (kg)
n	number of primary particles constituting an agglomerate or single particle (–)
q_m	specific charge (charge to mass ratio) (C/kg)
q	charge of primary particle (C)
q_∞	equilibrium charge of primary particle (C)
$\boldsymbol{r}$	particle position relative to its axis of rotation (m)
r_{ij}	distance between centroids of i-th and j-th particles (m)
$\boldsymbol{T}_d$	torque caused by rotational drag force (N·m)
$\boldsymbol{T}_p$	torque caused by the interaction between polarized primary particles (N·m)
$\boldsymbol{T}_q$	torque caused by the difference in Coulomb force of each primary particle (N·m)
t	time (s)
V_L	voltage applied to the lower electrode (V)
V_U	voltage applied to the upper electrode (V)
$\boldsymbol{v}_a$	velocity of agglomerate (m/s)
$\boldsymbol{v}_p$	velocity of particle (m/s)
x	horizontal or longitudinal direction
y	transverse direction perpendicular to the xz plane
z	direction perpendicular to the xy plane
z_p	particle position in the z-direction (m)
ε_0	vacuum permittivity = 8.85 × 10^{-12} (F/m)
ε_{rf}	relative permittivity of fluid (–)
ε_{rp}	relative permittivity of particle (–)
ε_{rs}	relative permittivity of solid (or particle layers) (–)
θ	angle of the agglomerate axis from the vertical (rad)
θ_{ex}	angle between external electric field direction and the vertical (rad)
θ_m	angle between the agglomerate axis and moving direction (rad)
κ	dynamic shape factor (–)
$\kappa_\perp$	dynamic shape factor perpendicular to moving direction (–)
$\kappa_{/\!/}$	dynamic shape factor parallel to moving direction (–)
μ	viscosity of fluid (Pa·s)
ρ_p	particle density (kg/m^3)
ρ_v	volume resistivity of particle (Ω·m)
τ	relaxation time (s)
φ	angle between the agglomerate axis and electric field direction (rad)
$\boldsymbol{\omega}$	angular velocity of agglomerate (rad/s)

subscripts

i	index for primary particle
r	radial direction
φ	circumferential direction

References

Adachi M., Maezono H., Kawamoto H., Sampling of regolith on asteroids using electrostatic force, Journal of Aerospace Engineering, 29 (2016) 04015081. DOI: 10.1061/(ASCE)AS.1943-5525.0000583

Adachi M., Hamazawa K., Mimuro Y., Kawamoto H., Vibration transport system for lunar and Martian regolith using dielectric elastomer actuator, Journal of Electrostatics, 89 (2017) 88–98. DOI: 10.1016/j.elstat.2017.08.003

Blajan M., Mizuno Y., Ito A., Shimizu K., Microplasma actuator for EHD induced flow, IEEE Transactions on Industry Applications, 59 (2017) 2409–2415. DOI: 10.1109/TIA.2016.2645160

Blanchard D.C., Electrically charged drops from bubbles in sea water and their meteorological significance, Journal of Meteorology, 15 (1958) 383–396. DOI: 10.1175/1520-0469(1958)015<0383:ECDFBI>2.0.CO;2

Calle C.I., Buhler C.R., McFall J.L., Snyder S.J., Particle removal by electrostatic and dielectrophoretic forces for dust control during lunar exploration missions, Journal of Electrostatics, 67 (2009) 89–92. DOI: 10.1016/j.elstat.2009.02.012

Cho A.Y.H., Contact charging of micron-sized particles in intense electric fields, Journal of Applied Physics, 35 (1964) 2561–2564. DOI: 10.1063/1.1713799

Dwari R.K., Mohanta S.K., Rout B., Soni R.K., Reddy P.S.R., Mishra B.K., Studies on the effect of electrode plate position and feed temperature on the tribo-electrostatic separation of high ash Indian coking coal, Advanced Powder Technology, 26 (2015) 31–41. DOI: 10.1016/j.apt.2014.08.001

Gotoh K., Mizutani K., Tsubota Y., Oshitani J., Yoshida M., Inenaga K., Enhancement of particle removal performance of high-speed air jet by setting obstacle in jet flow, Particulate Science Technology, 33 (2015) 567–571. DOI: 10.1080/02726351.2015.1060653

Hollmann H.E., Semiconductive colloidal suspensions with non-linear properties, Journal of Applied Physics, 21 (1950) 402–413. DOI: 10.1063/1.1699674

Hywel M., Green N.G., Dielectrophoretic manipulation of rod-shaped viral particles, Journal of Electrostatics, 42 (1997) 279–293. DOI: 10.1016/S0304-3886(97)00159-9

Kasper G., Niida T., Yang M., Measurements of viscous drag on cylinders and chains of spheres with aspect ratios between 2 and 50, Journal of Aerosol Science, 16 (1985) 535–556. DOI: 10.1016/0021-8502(85)90006-0

Kawamoto H., Some techniques on electrostatic separation of particle size utilizing electrostatic traveling-wave field, Journal of Electrostatics, 66 (2008) 220–228. DOI: 10.1016/j.elstat.2008.01.002

Kawamoto H., Shigeta A., Adachi M., Utilizing electrostatic force and mechanical vibration to obtain regolith sample from the moon and mars, Journal of Aerospace Engineering, 29 (2016) 04015031. DOI: 10.1061/(ASCE)AS.1943-5525.0000521

Kawamoto H., Uchiyama M., Cooper B.L., McKay D.S., Mitigation of lunar dust on solar panels and optical elements utilizing electrostatic traveling-wave, Journal of Electrostatics, 69 (2011) 370–379. DOI: 10.1016/j.elstat.2011.04.016

Klingenberg D.J., Swol F.V., Zukoski C.F., Dynamic simulation of electrorheological suspensions, The Journal of Chemical Physics, 91 (1989) 7888–7895. DOI: 10.1063/1.457256

Kobayakawa M., Kiriyama S., Yasuda M., Matsusaka S., Microscopic analysis of particle detachment from an obliquely oscillating plate, Chemical Engineering Science, 123 (2015) 388–394. DOI: 10.1016/j.ces.2014.11.046

Masuda H., Dry dispersion of fine particles in gaseous phase, Advanced Powder Technology, 20 (2009) 113–122. DOI: 10.1016/j.apt.2009.02.001

Masuda H., Gotoh K., Fukada H., Banba Y., The removal of particles from flat surfaces using a high-speed air jet, Advanced Powder Technology, 5 (1994) 205–217. DOI: 10.1252/kakoronbunshu.20.693

Masuda S., Fujibayashi K., Ishida K., Inaba H., Confinement and transportation of charged aerosol clouds via electric curtain, Electrical Engineering in Japan, 92 (1972) 43–52. DOI: 10.1002/eej.4390920106

Matsusaka S., Control of particle tribocharging, KONA Powder and Particle Journal, 29 (2011) 27–38. DOI: 10.14356/kona.2011007

Matsusaka S., Iyota J., Mizutani M., Yasuda M., Characterization and control of particles triboelectrically charged by vibration and external electric field, Journal of the Society of Powder Technology, Japan, 50 (2013) 632–639. DOI: 10.4164/sptj.50.632

Matsusaka S., Maruyama H., Matsuyama T., Ghadiri M., Triboelectric charging of powders: a review, Chemical Engineering Science, 65 (2010) 5781–5807. DOI: 10.1016/j.ces.2010.07.005

Matsusaka S., Yoshitani K., Tago H., Nii T., Masuda H., Iwamatsu T., Sampling of charged fine particles by motion control under AC field, Journal of the Society of Powder Technology, Japan, 45 (2008) 387–394. DOI: 10.4164/sptj.45.387

Mazumder M.K., Sharma R., Biris A.S., Zhang J., Calle C., Zahn M., Self-cleaning transparent dust shields for protecting solar panels and other devices, Particulate Science Technology, 25 (2007) 5–20. DOI: 10.1080/02726350601146341

Mizutani M., Yasuda M., Matsusaka S., Advanced characterization of particles triboelectrically charged by a two-stage system with vibrations and external electric fields, Advanced Powder Technology, 26 (2015) 454–461. DOI: 10.1016/j.apt.2014.11.021

Morgan H., Green N., Dielectrophoretic manipulation of rod-shaped viral particles, Journal of Electrostatics, 42 (1997) 279–293. DOI: 10.1016/S0304-3886(97)00159-9

Nader B.F., Castle G.S.P., Adamiak K., Effect of surface conduction on the dynamics of induction charging of particles, Journal of Electrostatics, 67 (2009) 394–399. DOI: 10.1016/j.

elstat.2008.12.017
Nakajima Y., Matsuyama T., Electrostatic field and force calculation for a chain of identical dielectric spheres aligned parallel to uniformly applied electric field, Journal of Electrostatics, 55 (2002) 203–221. DOI: 10.1016/S0304-3886(01)00198-X
Niida T., Ohtsuka S., Dynamic shape factors of regular shaped agglomerates and estimation based on agglomerate symmetry – for rectangular parallelepiped, V-and W-shaped, hexagonal and H-shaped agglomerates, KONA Powder and Particle Journal, 15 (1997) 202–211. DOI: 10.14356/kona.1997024
Ohkubo Y., Takahashi Y., Lifting criteria of an induction-charged spherical particle in a field with horizontally set parallel plate electrodes, Kagaku Kogaku Ronbunshu, 22 (1996a) 113–119. DOI: 10.1252/kakoronbunshu.22.113
Ohkubo Y., Takahashi Y., Experimental investigation on lifting criteria of an induction-charged spherical particle in a field with horizontally set parallel plate electrodes, Kagaku Kogaku Ronbunshu, 22 (1996b) 603–609. DOI: 10.1252/kakoronbunshu.22.603
Parthasarathy M., Klingenberg D.J., Electrorheology: mechanisms and models, Materials Science and Engineering, R17 (1996) 57–103. DOI: 10.1016/0927-796X(96)00191-X
Pearce C.A.R., The mechanism of the resolution of water-in-oil emulsions by electrical treatment, British Journal of Applied Physics, 5 (1954) 136–143. DOI: 10.1088/0508-3443/5/4/304
Shoyama M., Kawata T., Yasuda M., Matsusaka S., Particle electrification and levitation in a continuous particle feed and dispersion system with vibration and external electric fields, Advanced Powder Technology, 29 (2018) 1960–1967. DOI: 10.1016/j.apt.2018.04.022
Shoyama M., Matsusaka S., Electric charging of dielectric particle layers and levitation of particles in a strong electric field, Kagaku Kogaku Ronbunshu, 43 (2017) 319–326. DOI: 10.1252/kakoronbunshu.43.319
Shoyama M., Matsusaka S., Mechanism of disintegration of charged agglomerates in non-uniform electric field, Chemical Engineering Science, 198 (2019) 155–164. DOI: 10.1016/j.ces.2018.12.055
Shoyama M., Nishida S., Matsusaka S., Quantitative analysis of agglomerates levitated from particle layers in a strong electric field, Advanced Powder Technology, 30 (2019) 2052–2058. DOI: 10.1016/j.apt.2019.06.018
Tada T., Yamamoto T., Baba Y., Takeuchi M., Ion charging and electron charging to an insulating toner, Journal of the Society of Powder Technology, Japan, 41 (2004) 636–644. DOI: 10.4164/sptj.41.636
Washizu M., Jones T.B., Dielectrophoretic interaction of two spherical particles calculated by equivalent multipole-moment method, Conference Record of the 1994 IEEE, 2 (1994) 1483–1490. DOI: 10.1109/28.491470
Weber E., Electromagnetic Fields: Theory and Applications, Vol. I–Mapping of Fields, John Wiley & Sons, New York, 1950, pp. 215–233. DOI: 10.1063/1.3067394
Wu Y., Castle G.S.P., Inculet I.I., Petigny S., Swei G.S., Induction charge on freely levitating particles, Powder Technology, 135 (2003) 59–64. DOI: 10.1016/j.powtec.2003.08.004

Authors' Short Biographies

Mizuki Shoyama

Mizuki Shoyama is a Researcher of Chemical Engineering at Kyoto University. She earned her PhD from Kyoto University. She has worked as a development engineer in the aerospace division, IHI Corporation, and at Nuclear Fuel Industries, Ltd. Dr. Shoyama's current research interests include particle levitation on deposited particles with photoelectric charging and particle mixing using superimposed electric fields.

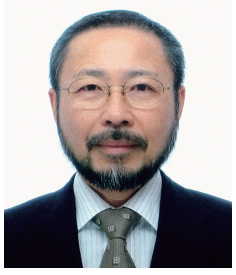

Shuji Matsusaka

Shuji Matsusaka is a Professor of Chemical Engineering at Kyoto University. He earned his PhD from Kyoto University. He has held important positions in academic organizations in areas of powder technology, aerosol science, and electrostatics. He is an emeritus editor-in-chief of *Advanced Powder Technology*. Dr. Matsusaka's current research interests include characterizing particle electrification, adhesion, and flowability, as well as the handling of micro-particles and nano-particles in gases.